Atmos. Chem. Phys. Discuss., 15, 18459–18485, 2015
www.atmos-chem-phys-discuss.net/15/18459/2015/
doi:10.5194/acpd-15-18459-2015

Atmospheric Chemistry and Physics Discussions
Open Access

Impact of future land cover changes on HNO_3 and O_3 surface dry deposition

T. Verbeke, J. Lathière, S. Szopa, and N. de Noblet-Ducoudré

Laboratoire des Sciences du Climat et de l'Environnement – LSCE-IPSL, CEA/CNRS/UVSQ, Gif-sur-Yvette, France

Received: 03 April 2015 – Accepted: 19 June 2015 – Published: 08 July 2015

Correspondence to: J. Lathière (juliette.lathiere@lsce.ipsl.fr)

Published by Copernicus Publications on behalf of the European Geosciences Union.

Abstract

Dry deposition is a key component of surface–atmosphere exchange of compounds, acting as a sink for several chemical species. Meteorological factors, chemical properties of the trace gas considered and land surface properties are strong drivers of dry deposition efficiency and variability. Under both climatic and anthropogenic pressure, the vegetation distribution over the Earth has been changing a lot over the past centuries, and could be significantly altered in the future. In this study, we perform a modeling investigation of the potential impact of land-cover changes between present-day (2006) and the future (2050) on dry deposition rates, with special interest for ozone (O_3) and nitric acid vapor (HNO_3), two compounds which are characterized by very different physico-chemical properties. The 3-D chemistry transport model LMDz-INCA is used, considering changes in vegetation distribution based on the three future projections RCPs 2.6, 4.5 and 8.5. The 2050 RCP 8.5 vegetation distribution leads to a rise up to 7 % (+0.02 $cm\,s^{-1}$) in VdO_3 and a decrease of −0.06 $cm\,s^{-1}$ in $VdHNO_3$ relative to the present day values in tropical Africa, and up to +18 and −15 % respectively in Australia. When taking into account the RCP 4.5 scenario, which shows dramatic land cover change in Eurasia, $VdHNO_3$ increases by up to 20 % (annual-mean value) and reduces VdO_3 by the same magnitude in this region. When analyzing the impact of dry deposition change on atmospheric chemical composition, our model calculates that the effect is lower than 1 ppb on annual mean surface ozone concentration, for both for the RCP8.5 and RCP2.6 scenarios. The impact on HNO_3 surface concentrations is more disparate between the two scenarios, regarding the spatial repartition of effects. In the case of the RCP 4.5 scenario, a significant increase of the surface O_3 concentration reaching locally up to 5 ppb (+5 %) is calculated on average during the June–August period. This scenario induces also an increase of HNO_3 deposited flux exceeding locally 10 % for monthly values. Comparing the impact of land-cover change to the impact of climate change, considering a 0.93 °C increase of global temperature, on dry deposition velocities, we estimate that the strongest increase over lands occurs in the North

Hemisphere during winter especially in Eurasia, by +50 % (+0.07 $cm\,s^{-1}$) for VdO_3 and +100 % (+0.9 $cm\,s^{-1}$) for $VdHNO_3$. However, different regions are affected by both changes, with climate change impact on deposition characterized by a latitudinal gradient, while the land-cover change impact is much more heterogeneous depending on vegetation distribution modification described in the future RCP scenarios. The impact of long-term land-cover changes on dry deposition is shown to be non-negligible and should be therefore considered in biosphere-atmospheric chemistry interaction studies in order to have a fully consistent picture.

1 Introduction

Amongst surface–atmosphere interactions, dry deposition plays a key role in and acts as a significant sink for several atmospheric compounds. Performing an intercomparison of 26 state-of-the-art atmospheric chemistry models, Stevenson et al. (2006) estimated the surface removal of ozone by dry deposition to be about 1000±200 $Tg\,yr^{-1}$ on average, with values ranging from 720 to 1507 $Tg\,yr^{-1}$ amongst models, compared to 5100, 4650 and 550 $Tg\,yr^{-1}$ for chemical production, chemical destruction and stratospheric input fluxes respectively. This study also underlined that although global deposition fluxes are consistent between models, locally, there is a large variability in the ozone deposition velocities (Stevenson et al., 2006). Since all these models use deposition schemes based on Wesely's prescription, the discrepancies suggest different hypotheses for the land-type consideration. Based on satellite measurements from OMI (Ozone Monitoring Instrument) combined with the Goddard Earth Observing System chemical transport model (GEOS-Chem), Nowlan et al., 2014 estimated dry deposition to land to be 98 % of total deposition for NO_2 and 33 % for SO_2. This deposition fluxes over land represent 3 % of global NO_x emissions and 14 % of global *S* emissions. Land surfaces can therefore play a significant role on deposition, with a higlhy variable contribution depending on the chemical compound considered/from one chemical compound to another.

ACPD
15, 18459–18485, 2015

The air–surface exchange of trace compounds has been shown to be strongly variable, especially between different types of surface vegetation and soil characteristics (Wesely et al., 2000). Regarding ozone, model data differences reported in the literature could be attributed to oversimplifications in the implementation of the dry deposition scheme (Val Martin et al., 2014).

In order to quantify the non-photochemical sink for tropospheric burden at regional and global scale, the scientific community has developed numerical dry deposition schemes calibrated with field-measurements of dry deposition velocities (Wesely et al., 1989; Zhang et al., 2002), implemented usually in chemistry-transport models. Dry deposition efficiency is influenced by multiple meteorological factors (temperature, solar radiation, humidity), chemical properties of the trace gas considered (solubility, oxidative capacity), and land surface properties (surface type, surface roughness, foliar surface and ecosystem height in the case of vegetation surfaces). Some of these factors are poorly constrained and are thus accounted for in deposition schemes in an very simplistic way. The vegetation distribution for instance is usually prescribed using maps for the region of interest that are usually kept the same for either past, present or future studies. There is therefore a lack of knowledge regarding the impact of long-term changes in vegetation distribution on dry deposition chemical compounds at the surface. Dry deposition parameters (resistances, fluxes, etc.) being especially tricky to measure, it limits the evaluation of dry deposition schemes, especially at the global scale for which a variety of surface and meteorological conditions should be documented. And yet, since the beginning of industrial era, human activities have modified the use of large surfaces, affecting significantly the vegetation distribution, especially in the northern temperate latitude regions. Land cover modifications are expected in the 21st century due to projected increases in energy and food demands. Vegetation in tropical regions in particular could undergo drastic alterations.

The objective of this study is to investigate the potential impact of land-cover changes between present-day (2006) and the future (2050) on dry deposition rates, using a modeling approach with a 3-D chemistry transport model. Changes in vegetation distribution are based on the three future projections known as Representative Concentration Pathways scenarios (RCPs) (van Vuuren et al., 2011), developed for the climate model intercomparison project (CMIP5): RCPs 2.6, 4.5 and 8.5. For this work we focus on ozone (O_3) and nitric acid vapor (HNO_3), two compounds which are characterized by very different biophysical properties (e.g. solubility and oxidant capacity). In Sect. 2, we describe the chemistry-transport model LMDz-INCA, the dry deposition module and the modeling strategy adopted. In Sect. 3, we describe the different future land cover changes as given in the 3 RCP scenarios 2.6, 4.5 and 8.5, and explain their impacts on dry deposition velocities of ozone and nitric acid vapor. Finally, the magnitude of land cover effects related to climate change by 2050 is discussed.

2 Modeling set up

In our study, the global chemistry-climate model LMDz-INCA (Hauglustaine et al., 2004) is used to compute dry deposition. LMDz (v4) is an atmospheric general circulation model that simulates the transport of trace species. The model is run with 19 hybrid levels from the surface to 3 hPa at a horizontal resolution of 1.85° in latitude and 3.75° in longitude. It is coupled on-line to the chemistry and aerosols model INCA (v2) which computes concentrations of reactive tracers considering their emissions, chemical transformations, transport and deposition processes. The atmospheric oxidation reactions of CH_4, CO and non-methane hydrocarbons are documented in Folberth et al. (2006). Emissions are prescribed according to Lamarque et al. (2010) for anthropogenic fluxes and Lathière et al. (2006) for biogenic VOCs, as described in Szopa et al. (2013).

2.1 Dry deposition in LMDz-INCA

The chemical deposition scheme used in INCA is based on the parameterization of Wesely (1989) and Wesely and Hicks (2000), computing dry deposition velocity Vd as

ACPD
15, 18459–18485, 2015

a succession of resistances as follows:

$$|V_\mathrm{d}| = [R_\mathrm{a} + R_\mathrm{b} + R_\mathrm{c}]^{-1} \quad (1)$$

where R_a is the aerodynamic resistance (influenced by atmospheric stability and wind speed above the canopy), R_b is the quasi-laminar resistance (controlled by molecular diffusivity), and R_c is the bulk surface resistance (depending on both surface and trace gas properties).

The surface resistance R_c especially depends on specific surface (roughness length) (Wesely, 1989) and meteorological (temperature and solar radiation) parameters. The surface occupancy type (presence of urban sites, water, vegetation, etc.) strongly modulates those parameters. In particular vegetation surfaces cover a large area of the Earth, with a high spatial and seasonal variability due to species diversity and functioning, and are a key factor in dry deposition determination. The dry deposition scheme implemented in LMDz-INCA considers eleven surface categories: (1) urban land, (2) agricultural land, (3) range land, (4) deciduous forest, (5) coniferous forest, (6) mixed forest including wetland, (7) water, both salt and fresh, (8) barren land, mostly desert, (9) non-forested wetland, (10) mixed agricultural and range land, and (11) rock open areas with low-growing shrubs. This scheme was originally developed by Wesely (1989) and updated by Wesely and Hicks (2000) for Northern Hemisphere regions of United States and southern Canada regions. Five seasonal categories are used as proxy of vegetation growth stage (midsummer with lush vegetation; autumn with unharvested cropland; late autumn after frost, no snow; winter, snow on ground, and subfreezing; transitional spring with partially green short annuals). For global scale study purposes, the scheme in LMDz-INCA has been modified in order to represent the different seasonal cycles throughout the world. The latitude dependency of the vegetation seasonality is described by dividing the globe into three belts: Northern Hemisphere regions (latitude $> 33^\circ$ N); Tropical regions (33° S $<$ latitude $< 33^\circ$ N) and Southern Hemisphere regions (latitude $< 33^\circ$ S). Summer is considered in the tropics throughout the whole year, describing the evergreen vegetation. Two opposite seasonal cycles are taken into

ACPD
15, 18459–18485, 2015

account in extra-tropical Northern and Southern Hemisphere regions, with winter being activated when snow falls. The dry deposition velocity over each grid box is eventually determined by summing deposition velocities computed over every land cover types, weighted by their respective fractional surface coverage (ranging from 0 to 1).

The deposition rates computed by LMDz-INCA are consistent with typical deposition velocities exposed for North America and Europe presented in Wesely and Hicks (2000) and more generally with global models with monthly values reaching up to $0.6\,\mathrm{cm\,s^{-1}}$ for ozone and up to $3\,\mathrm{cm\,s^{-1}}$ for HNO_3 over land.

2.2 Land use and land cover changes between 2007 and 2050

The present-day distribution of vegetation categories considered in LMDz-INCA is illustrated in Fig. 1 as dominant type, covering the largest fraction of each gridbox. Crops are dominant mainly in restricted temperate regions of North America, Central Europe, and also in India, while range lands are largely spread. Deciduous forests dominate in tropical regions of South America, Africa and Indonesia, together with Central and Southern Europe, while coniferous forests have a high occupancy in boreal regions of North America and Eurasia. The Fig. 1 also shows the 10 regions of special interest selected for this study, that will be considered in more details when analyzing our results.

Future maps are based on scenarios of land-cover changes derived from four different Representative Concentration Pathways (RCPs; Moss et al., 2010; Van vuuren et al., 2011) and four Integrated Assessment Models (one per RCP) (RCP 8.5, RCP 4.5 and RCP 2.6). Those maps were further harmonized to ensure smooth transitions with past/historical changes (Hurtt et al., 2011). Those datasets only provide information on human activities (crop land and grazed pastureland) in each grid-cell (at a 0.5° resolution) but do not provide any recommendation regarding the distribution of natural vegetation. We have therefore combined them with our original present-day land-cover map (Loveland et al., 2000), which already includes both natural and anthropogenic vegetation types, following a methodology described in Dufresne et al. (2013).

ACPD
15, 18459–18485, 2015

Figure 2 illustrates changes in vegetation fraction for agriculture and grasslands on one hand, and for forests on the other hand, between present-day and the future RCP scenarios. For most affected regions, the changes in land surfaces are presented in Fig. 3. The RCP 4.5 scenario shows the largest surface change with a total of 20.8×10^6 km^2, representing 10.4 % of the 70° S–70° N Earth continental surface. According to the RCP 2.6 and RCP 8.5 scenarios only 15 to 16.8×10^6 km^2 of land cover surfaces are converted.

The RCP 2.6 scenario is characterized by a moderate increase of energy consumption throughout the 21st century together with a decrease in oil consumption. The energy supply is thus partly ensured by bioenergy production increase (van Vuuren et al., 2011). Such hypotheses lead to a strong expansion of agricultural lands ($+2.61 \times 10^6$ km^2 globally) at the expense of forests (-1.40×10^6 km^2) and grasslands (-1.15×10^6 km^2) targeting mainly Eurasia, US and tropical southern America.

The RCP 8.5 scenario, characterized by the strongest increase in population and energy consumption (amongst RCPs), assumes a large increase in global population until 2050. The resulting demand for food leads to a strong expansion of land used for crops and pastures at the expense of forests. The tropical belt (from 30° N to 30° S) undergoes the largest changes: tropical forests in southern America and southern Africa are partially harvested (1.0×10^6 km^2 totally, i.e. 13 % of their 2007 extent) and replaced by grassland and crops, while in Eastern Australia, forests lose 7 % (-0.28×10^6 km^2) of their 2007 area and are replaced by grasslands which gains 0.12×10^6 km^2 on desert.

The "mitigation" RCP 4.5 scenario is a rather contrasting scenario as it proposes a strong increase in all forests' occupancy, a small expansion of grasslands but an important recession of agricultural surfaces mainly in developed countries. Indeed Eurasia and US and Canada undergo a strong conversion from agriculture and grassland to forests with a magnitude change of $\sim 0.8 \times 10^6$ km^2 in Eurasia and $\sim 0.4 \times 10^6$ km^2 in northern US and Canada. Besides, tropical southern America losses 0.55×10^6 km^2 of cumulated croplands and grasslands but forests expand by the same surface between present day and 2050.

ACPD
15, 18459–18485, 2015

2.3 Simulation strategy

In order to quantify the effects of these land cover changes on dry deposition, we carried out two sets of simulations (Table 1). The first set intends to isolate the effect of future possible land cover changes on dry deposition prior to any climate change. It includes one control run (present day), using 2006 vegetation distribution (Fig. 1) and three future runs using the 2050 vegetation maps according to the RCPs 8.5, 4.5 and 2.6 scenarios. The same present-day meteorology, biogenic and anthropogenic emissions are used in these four simulations. These simulations are run for 1 year with wind and temperature fields being relaxed towards the ECMWF ERA-interim reanalysis (Dee et al., 2011) with a time constant of 6 h.

Then a second set of two simulations is performed in order to investigate the effect of future climate change on deposition and compare it with the impact of future land cover change: one run for the 2000–2010 period and a second run for the 2045–2055 period. Those simulations are performed without nudging and the LMDz general circulation model requires sea surface temperature (SST), solar constant and Long-Lived Green House Gases (LL-GHG) global mean concentrations as forcings. For historical simulations, we use the HADiSST for sea surface temperature (Rayner et al., 2003) and the evolution of LL-GHG concentrations compiled in the AR4-IPCC report. For future projections, we use the SST from IPSL-CM4 simulation for the SRES-A2 scenario, which induce similar climate trajectories in terms of radiative forcing than RCP8.5. We use the LL-GHG concentrations distributed by the RCP database for RCP8.5 projection for the 2045–2055 period. Eleven years are run and averaged to allow smoothing of interannual climate variability. The mean surface temperature changes is 0.93 °C between future simulation and present day simulation. Both experiments use the same present-day vegetation distribution, anthropogenic and biogenic emissions.

ACPD
15, 18459–18485, 2015

3 Results

3.1 Present day ozone and nitric acid deposition

First of all, we present the deposition over continental regions for present-day conditions (Fig. 4) by illustrating the annual means of deposition rates, surface concentrations and deposited fluxes for O_3 and HNO_3.

The highest ozone deposition velocities ($> 0.35\,cm\,s^{-1}$) are simulated over India, south-eastern Asia, western coast and center of south America, Mexico, Europe and sub saharian Africa and Australia. Hence, those areas are mainly covered by crops and grasses, where the highest VdO_3 occurs, while Europe and Southeast Asia are mainly covered by deciduous forests, with therefore lower VdO_3. O_3 dry deposition is indeed maximal over small canopies vegetation and minimal over bare soil with deposition affinity ranging from Agriculture > Grasslands > Deciduous > Coniferous > Bare soil (see sensitivity tests in Supplement).

Temperate regions see ozone deposition velocities significantly reduced in winter (see Supplement for monthly means) whereas tropical regions, covered mainly by small canopies, are characterized by deposition rate exceeding $0.35\,cm\,s^{-1}$ throughout the whole year due to the lack of seasonality in the vegetation phenology in the global model. In temperate regions of the Northern Hemisphere, the highest values of deposition velocity for both ozone reaching monthly mean values of 0.4 to $0.6\,cm\,s^{-1}$ for VdO_3 over Europe.

For HNO_3, the annual mean deposition rates are maximum over Brazil, Western Europe, India, Indochinese Peninsula and South of western Africa ($> 1.6\,cm\,s^{-1}$ in annual mean). $VdHNO_3$ reaches maximum values over deciduous and coniferous forests, due to deposition affinity ranking from: Deciduous, Coniferous > Agriculture > Grasslands > Bare soil. This is due to the strong dependency of $VdHNO_3$ to surface roughness (Walcek et al., 1986). For temperate region and South Asia, the HNO_3 deposition is strongly affected by the vegetation cycle with maximum in

ACPD
15, 18459–18485, 2015

July between 2.5 and 3.5 $cm\,s^{-1}$. This is remarkable over temperate and boreal forests. In the tropics, Amazonian forest encounters high HNO_3 deposition rate in January whereas deposition rate over African equatorial forest is limited throughout the whole year. (see Supplement for monthly means of deposition).

The repartition of deposited fluxes is strongly affected by the large variability of atmospheric concentrations of ozone and nitric acid in the surface layer. For both O_3 and HNO_3, the deposited fluxes are maximum over South and East Asia and eastern North America and central and western Europe. For ozone, the maximum in January is over central Africa whereas in July the ozone deposition is maximum over central Europe and eastern US. For HNO_3, the deposited flux repartition mixes more the deposition rate and the HNO_3 surface concentrations heterogeneities. In January, HNO_3 is maximally deposited over eastern US, central Africa, central Europe India and East Asia. In July, regions are the same in the Northern Hemisphere but the extension of deposited HNO_3 areas is higher and the deposition in Africa is weak, due to weak HNO_3 concentration.

3.2 Impact of 2050–2007 land cover changes on dry deposition velocities

We then analyze the changes in dry deposition velocities between present day and 2050 induced only by land cover changes. Four regions undergo interesting land cover changes in term of intensity or contrast between scenarios: Eurasia, North America, tropical Africa and Australia. The left columns of Figs. 5 and 6 show the relative difference in dry deposition velocities distribution for O_3 and HNO_3, resulting from the changes in vegetation distribution between 2007 and 2050 for the 3 RCP scenarios. We shall first describe the two scenarios projecting weak land cover changes for 2050s: RCP8.5 and RCP2.6. In the RCP 8.5 scenario, one main land cover change is the expansion of agricultural land at the expenses of forests. According to this scenario, over tropical Africa, the maximal land cover change occurs locally with fraction of deciduous forests decreasing up to 0.2 while cropland fraction increases by up to 0.2 in the

ACPD
15, 18459–18485, 2015

same region. This induces a rise up to 7 % (+0.02 $cm\,s^{-1}$) in VdO_3 and a decrease of −0.06 $cm\,s^{-1}$ in $VdHNO_3$ relative to the present day values in this area. These order of magnitude and sign of changes are consistent with sensitivity tests in which we replaced totally forests by croplands inducing an increase of 0.1 $cm\,s^{-1}$ in VdO_3 and a decrease of 0.5 $cm\,s^{-1}$ in $VdHNO_3$ (during summer and winter). The strongest LCC occurs in Australia (−0.12 in forest fraction and +0.2 in grassland fraction in eastern Australian regions), which induces a local maximum increase of 18 % (+0.05 $cm\,s^{-1}$) in VdO_3 and a maximum decrease of 15 % in $VdHNO_3$ (−0.1 $cm\,s^{-1}$). We find the same order of magnitude in changes induced by land cover change in Western Australia but with a different sign for $VdHNO_3$ changes (+0.1 $cm\,s^{-1}$; +9 %), due to a different type of shift in surface covering (+0.12 in grassland fraction, −0.10 for desert).

As land cover changes are weak in the RCP 2.6 scenario, a more dispersed and weaker effect on dry deposition velocities is simulated (maximum absolute difference of 10 %).

According to the RCP 4.5 scenario, the most dramatic land cover change occurs in Eurasia where local maximum changes of up to 0.5 in fraction of vegetation are projected, involving in most cases an increase in forest surface at the expense of agricultural area. This increases $VdHNO_3$ by up to 20 % (annual-mean value) and reduces VdO_3 by the same magnitude in this region. The LCC impacts are stronger by a factor 4 to 6 in summer both on O_3 and HNO_3 deposition rates. This difference in deposition velocities between winter and summer were highlighted in sensitivity tests which see a strong decrease in VdO_3 during the June–August period (up to 0.15 $cm\,s^{-1}$ in absolute) and a strong increase in $VdHNO_3$ (up to 1.5 $cm\,s^{-1}$) underlining a total conversion of croplands to forests. This is due to a higher surface roughness which enhances the deposition velocity of HNO_3 (via the reduction of the aerodynamic resistance). However, the higher input surface resistance (prescribed in the model and variable relating to season indexes) reduces VdO_3 even combined to a warmer climate which decreases the stomatal resistance.

ACPD
15, 18459–18485, 2015

3.3 Impact on atmospheric composition

The objective of this part is to isolate the effects of dry deposition changes due to land cover changes on the tropospheric concentration of O_3 and HNO_3. Therefore, solely the impact of land cover changes on deposition is considered between the present-day and 2050 simulations. This impact on surface concentrations of O_3 and HNO_3 is shown in the right columns of Figs. 5 and 6.

For both the RCP8.5 and RCP2.6 scenarios, the LLC effects through deposition are lower than 1 ppb on annual mean surface ozone concentrations. In term of relative difference, only the reduction of ozone over Australia when considering RCP8.5 hypotheses is exceeding 1 %, reaching up to 5 % at some points. The impact on HNO_3 surface concentrations is more disparate between the two scenarios when considering the spatial repartition of effects. The RCP8.5 lead to local increase of HNO_3 due to the reduction of deposition rate. This HNO_3 increase is notable over Mexico, Brazil, western and South Africa (comprised in the 1–6 %interval). Land cover change in Australia leads to an increase exceeding 7 % on the eastern part and a decrease reaching 5 % on the western part.

The RCP4.5 scenario induces the strongest impacts on deposition rate with a reduction of VdO_3 ($-0.08\,\mathrm{cm\,s^{-1}}$) occurring in Eurasia due a strong reduction in croplands occupancy (−0.6 in fraction of coverage) and a strong increase in forest distribution (+0.6 in fraction of coverage) between 2007 and 2050. It induces a significant increase of the surface O_3 concentration reaching locally up to 5 ppb (+5 %) on average during the June–August period. This scenario induces also an increase of HNO_3 deposited flux exceeding locally 10 % for monthly values. In Eurasia and eastern North America. It thus leads to reduction in HNO_3 concentration of 0.2 ppb in Eurasia (−13 %) and in North America (−8 %) via changes in nitric acid vapor velocities of $+0.5\,\mathrm{cm\,s^{-1}}$ and +0.2 respectively.

ACPD
15, 18459–18485, 2015

3.4 Are the land cover induced changes significant compared with the climate change impact?

The impact of land-use changes on deposition can be compared to the one of climate in order to discuss their respective strength on deposition rates. In this purpose, we consider a 0.93 °C increase of global temperature, corresponding to the temperature increase planned in RCP projections between the beginning and the middle of the 21st century. The Fig. 7 shows the impact of this climate change on deposition rate for O_3 and HNO_3. We see that the strongest increase in dry deposition velocities over lands occurs in the North Hemisphere during winter especially in Eurasia (+50 % ($+0.07\,cm\,s^{-1}$) for VdO_3 and +100 % ($+0.9\,cm\,s^{-1}$) for $VdHNO_3$). The climate effect on deposition rate by affecting stomatal resistance, sensitive to surface temperature and solar radiance, can locally reach values far more important than the LCC. The Table 2 presents the effects of land cover change considering RCP4.5 projection and climate change on deposition rate averaged over 10 regions for O_3 and HNO_3. In several regions, the effect of land cover change is of the same order of magnitude than the one of climate. The modification in land cover affectation can thus amplify the climate change effect or, when the sign is the opposite, counterbalances it.

4 Conclusion and discussion

Using the 2.6, 4.5 and 8.6 RCP scenarios for land-use change between 2000s and 2050s, simulations were carried out with the global chemistry-transport model LMDz-INCA in order to assess to impact of changes in vegetation distribution on the dry deposition of ozone and nitric acid at the surface and on atmospheric composition.

Regarding vegetation distribution, the largest change at the global scale is given in the RCP 4.5 scenario ($20.8 \times 10^6\,km^2$), with surface converted being 28 and 19 % lower in the RCP 2.6 and RCP 8.5 scenarios respectively. Projections show major changes in the Northern Hemisphere in the case of RCP 4.5 scenario, while Australia and Africa are mostly affected in the RCP 8.5 scenario.

Vegetation type and surface being key drivers of surface dry deposition, any change in vegetation distribution can potentially affect dry deposition velocity and therefore atmospheric chemical composition. Considering the 2050 RCP 8.5 vegetation distribution leads to a rise up to 7 % (+0.02 $cm\,s^{-1}$) in VdO_3 and a decrease of −0.06 $cm\,s^{-1}$ in $VdHNO_3$ relative to the present day values in tropical Africa, and up to +18 and −15 % respectively in Australia. As land cover changes are weak in the RCP 2.6 scenario, a more dispersed and weaker effect on dry deposition velocities is simulated (maximum absolute difference of 10 %) when considering the RCP 2.6 scenario, characterized by a moderate change in vegetation distribution compared to present-day. When taking into account the RCP 4.5 scenario, which shows dramatic land cover change in Eurasia $VdHNO_3$ increases by up to 20 % (annual-mean value) and reduces VdO_3 by the same magnitude in this region. When analyzing the impact of dry deposition change on atmospheric chemical composition, our model calculates that the effect is lower than 1 ppb at the grid box scale on annual mean surface ozone concentration, for both for the RCP8.5 and RCP2.6 scenarios. The impact on HNO_3 surface concentrations is more disparate between the two scenarios, regarding the spatial repartition of effects. In the case of the RCP 4.5 scenario, a significant increase of the surface O_3 concentration reaching locally up to 5 ppb (+5 %) is calculated on average during the June–August period. This scenario induces also an increase of HNO_3 deposited flux exceeding locally 10 % for monthly values. Investigating the impact of climate change, considering a 0.93 °C increase of global temperature, on dry deposition velocities, we calculate see that the strongest increase over lands occurs in the North Hemisphere during winter especially in Eurasia (+50 % (+0.07 $cm\,s^{-1}$) for VdO_3 and +100 % (+0.9 $cm\,s^{-1}$) for $VdHNO_3$). The climate change impact on deposition is characterized by a latitudinal gradient, while the effect of land-cover change is much more heterogeneous. Both climate and vegetation distribution changes are of similar amplitude but sign can differ.

Vegetation is usually crudely described in chemistry-transport models, with leaf surface or cuticle and stomatal resistances for instance being prescribed or very simply parameterized, and lack of representation of seasonal variation or stress (water, temperature) impacts. This could lead to significant uncertainty in model representation and projections of atmospheric chemical composition and surface–atmosphere interactions. The work by Wesely and Hicks (2000) underlines that selecting proper input parameters of dry deposition scheme, such as stomatal, cuticle, and soil resistances, is crucial for a satisfactory determination of dry deposition efficiency, for both simple and multi-layers models. Investigating the impact of coupling dry deposition to vegetation phenology in the Community Earth System Model (CESM) on ozone surface simulation, Val Martin et al. (2014) shows the importance of representing the dependence of dry deposition to vegetation parameters including drivers of stomatal resistance variation (change in CO_2, drought stress), especially when focusing on the impact of past or future changes of vegetation. Next generation of chemistry-transport models should therefore rely on online coupling with vegetation, with dry deposition schemes having a consistent and dynamic description of vegetation distribution and growth and related short-term (seasonal, annual variation) or long-term (past and future changes) evolutions.

The Supplement related to this article is available online at doi:10.5194/acpd-15-18459-2015-supplement.

Acknowledgements. Computer time was provided by the GENCI French supercomputing program. This research was supported by CNRS, via the INSU-LEFE French Program under the project BOTOX.

ACPD
15, 18459–18485, 2015

Title Page
Abstract | Introduction
Conclusions | References
Tables | Figures
◂◂ | ▸▸
◂ | ▸
Back | Close
Full Screen / Esc
Printer-friendly Version
Interactive Discussion

References

Folberth, G., Hauglustaine, D. A., Ciais, P., and Lathière, J.: On the role of atmospheric chemistry in the global CO_2 budget, Geophys. Res. Lett., 32, L08801, doi:10.1029/2004GL021812, 2005.

Hauglustaine, D. A., Hourdin, F., Jourdain, L., Filiberti, M. A., Walters, S., Lamarque, J.-F., and Holland, E. A.: Interactive chemistry in the Laboratoire de Meteorologie Dynamique general circulation model: description and background tropospheric chemistry evaluation, J. Geophys. Res.-Atmos., 109, D04314, doi:10.1029/2003JD003957, 2004.

Hurtt, G. C., Fisk, J., Thomas, R. Q., Dubayah, R., Moorcroft, P. R., and Shugart, H. H.: Linking models and data on vegetation structure, J. Geophys. Res.-Biogeo., 115, G00E10, doi:10.1029/2009JG000937, 2010.

Hurtt, G. C., Chini, L. P., Frolking, S., Betts, R. A., Feddema, J., Fischer, G., Fisk, J. P., Hibbard, K., Houghton, R. A., Janetos, A., Jones, C. D., Kindermann, G., Kinoshita, T., Klein Goldewijk, K., Riahi, K. Shevliakova, E., Smith, S., Stehfest, E., Thomson, A., Thornton, P., van Vuuren, D. P., and Wang, Y. P.: Harmonization of land-use scenarios for the period 1500–2100: 600 years of global gridded annual land-use transitions, wood harvest, and resulting secondary lands, Climatic Change, 109, 117–161, doi:10.1007/s10584-011-0153-2, 2011.

Lathière, J., Hauglustaine, D. A., De Noblet-Ducoudré, N., Krinner, G., and Folberth, G. A.: Past and future changes in biogenic volatile organic compound emissions simulated with a global dynamic vegetation model, Geophys. Res. Lett., 32, L20818, doi:10.1029/2005GL024164, 2005.

Moss, R. H., Edmonds, J. A., Hibbard, K. A., Manning, M. R., Rose, S. K., van Vuuren, D. P., Carter, T. R., Emori, S., Kainuma, M., Kram, T., Meehl, G. A., Mitchell, J. F., Nakicenovic. N., Riahi, K., Smith, S. J., Stouffer, R. J., Thomson, A. M., Weyant, J. P., and Wilbanks, T. J.: The next generation of scenarios for climate change research and assessment, Nature, 463, 747–756, doi:10.1038/nature08823, 2010.

Nowlan, C. R., Martin, R. V., Philip, S., Lamsal, L. N., Krotkov, N. A., Marais, E. A., Wang, S., and Zhang, Q.: Global dry deposition of nitrogen dioxide and sulfur dioxide inferred from space-based measurements, Global Biogeochem. Cy., 28, 1025–1043, doi:10.1002/2014GB004805, 2014.

Rayner, N. A., Parker, D. E., Horton, E. B., Folland, C. K., Alexander, L. V., Rowell, D. P., Kent, E. C., and Kaplan, A.: Global analyses of sea surface temperature, sea ice, and night

ACPD
15, 18459–18485, 2015

Impact of future land cover changes on HNO_3 and O_3 surface dry deposition

T. Verbeke et al.

marine air temperature since the late nineteenth century, J. Geophys. Res.-Atmos., 108, 2156–2202, doi:10.1029/2002JD002670, 2003.
Stevenson, D. S., Dentener, F. J., Schultz, M. G., Ellingsen, K., van Noije, T. P. C., Wild, O., Zeng, G., Amann, M., Atherton, C. S., Bell, N., Bergmann, D. J., Bey, I., Butler, T., Cofala, J., Collins, W. J., Derwent, R. G., Doherty, R. M., Drevet, J., Eskes, H. J., Fiore, A. M., Gauss, M., Hauglustaine, D. A., Horowitz, L. W., Isaksen, I. S. A., Krol, M. C., Lamarque, J. F., Lawrence, M. G., Montanaro, V., Muller, J.-F., Pitari, G., Prather, M. J., Pyle, J. A., Rast, S., Rodriguez, J. M., Sanderson, M. G., Savage, N. H., Shindell, D. T., Strahan, S. E., Sudo, K., and Szopa, S.: Multimodel ensemble simulations of present-day and near-future tropospheric ozone, J. Geophys. Res.-Atmos., 111, D08301, doi:10.1029/2005JD006338, 2006.
Szopa, S., Balkanski, Y., Schulz, M., Bekki, S., Cugnet, D., Fortems-Cheiney, A., Turquety, S., Cozic, A., Deandreis, C., Hauglustaine, D., Idelkadi, A., Lathière, J., Lefèvre, F., Marchand, M., Vuolo, R., Yan, N., and Dufresne, J.-L.: Aerosol and ozone changes as forcing for climate evolution between 1850 and 2100, Clim. Dynam., 40, 2223–2250, doi:10.1007/s00382-012-1408-y, 2013.
Val Martin, M., Heald, C. L., and Arnold, S. R.: Coupling dry deposition to vegetation phenology in the Community Earth System Model: implications for the simulation of surface O_3, Geophys. Res. Lett., 41, 2988–2996, doi:10.1002/2014GL059651, 2014.
van Vuuren, D. P., Edmonds, J., Kainuma, M., Riahi, K., Thomson, A., Hibbard, K., Hurtt, G. C., Kram, T., Krey, V., Lamarque, J.-F., Masui, T., Meinshausen, M., Nakicenovic, N., Smith, S. J., and Rose, S. K.: The representative concentration pathways: an overview, Climatic Change, 109, 5–31, doi:10.1007/s10584-011-0148-z, 2011.
Wesely, M. L.: Parameterization of surface resistances to gaseous dry deposition in regional-scale numerical models, Atmos. Environ., 23, 1293–1304, doi:10.1016/0004-6981(89)90153-4, 1989.
Wesely, M. L. and Hicks, B. B.: A review of the current status of knowledge on dry deposition, Atmos. Environ., 34, 2261–2282, doi:10.1016/S1352-2310(99)00467-7, 2000.
Zhang, L. M., Moran, M. D., Makar, P. A., Brook, J. R., and Gong, S. L.: Modelling gaseous dry deposition in AURAMS: a unified regional air-quality modelling system, Atmos. Environ., 36, 537–560, doi:10.1016/S1352-2310(01)00447-2, 2002.

ACPD
15, 18459–18485, 2015

Table 1. Simulations performed in our study with the LMDz-INCA chemistry-climate model: set-up description.

Run objectives	Land-cover map	Climate	Duration
Control	Present-day 2000s	Winds and surface temperature nudged on ECMWF fields for 2007	1 year
Impact of future land-use changes	2050 RCP 8.5 2050 RCP 4.5 2050 RCP 2.6	Winds and surface temperature nudged on ECMWF fields for 2007	1 year
Impact of future climate	Present-day 2000s	2000–2010 fields (GCM mode) 2045–2055 fields (GCM mode)	10 years

ACPD
15, 18459–18485, 2015

Table 2. Mean Effect on Annual Mean Deposition Rate (%) of climate and land cover changes of O_3 and HNO_3 averaged over homogeneous regions (values > ±1.5 % are highlighted).

	Ozon			Nitric Acid		
	Climate Change	RCP4.5 Land cover Change	Sum of Climate and Land cover Changes	Climate Change	RCP4.5 Land cover Change	Sum of Climate and Land cover Changes
GLOBAL	0.5	−0.7	−0.2	*2.2*	1.2	*3.4*
Eurasia	***2.1***	*−2.1*	0.0	*4.3*	*3.8*	*8.1*
USA	**1.5**	−1.3	0.2	*3.6*	*2.0*	*5.6*
Central America	−1.1	−1.4	*−2.6*	1.1	*1.7*	*2.8*
Tropical Southern America	***−2.3***	−1.2	*−3.5*	1.1	*2.6*	*3.7*
Tropical Africa	***−1.5***	−0.8	*−2.3*	0.4	0.9	1.3
South Africa	−1.4	−0.6	*−2.0*	−0.1	0.8	0.8
West Australia	−0.4	−0.1	−0.5	−0.4	0.0	−0.4
East Australia	−0.5	−0.6	−1.1	0.2	0.5	0.7
South America	0.4	−0.7	−0.4	0.3	*2.0*	*2.3*
Tropics	−1.1	−0.6	*−1.7*	0.6	1.0	*1.7*

ACPD
15, 18459–18485, 2015

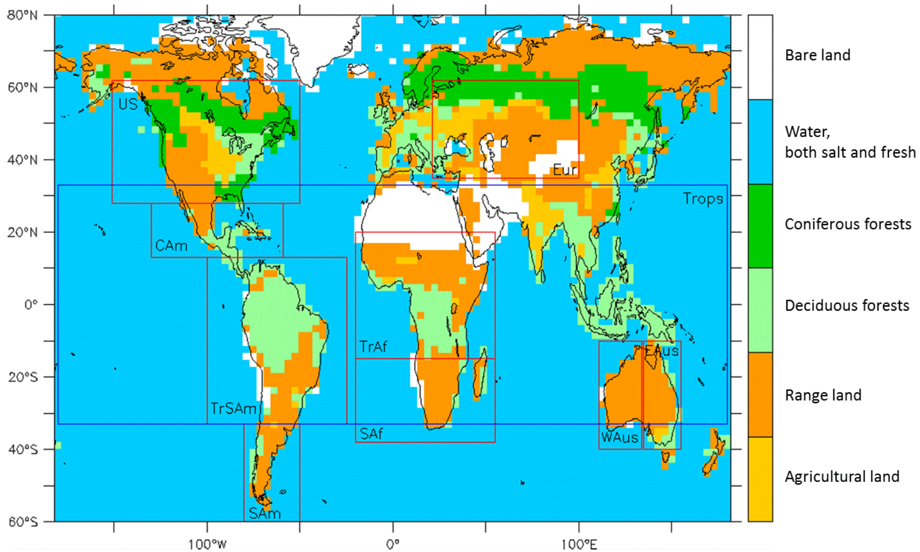

Figure 1. Surface categories considered in LMDz-INCA for dry deposition, represented as dominant coverage: agricultural land, range land, deciduous forest, coniferous forest, water, barren land, mostly desert. Regions discussed in this study are also illustrated: Eurasia, USA, Central America, Tropical Southern America, Southern America, Tropical Africa, Southern Africa, Western Australia, Eastern Australia and Tropical regions.

ACPD
15, 18459–18485, 2015

Impact of future land cover changes on HNO_3 and O_3 surface dry deposition

T. Verbeke et al.

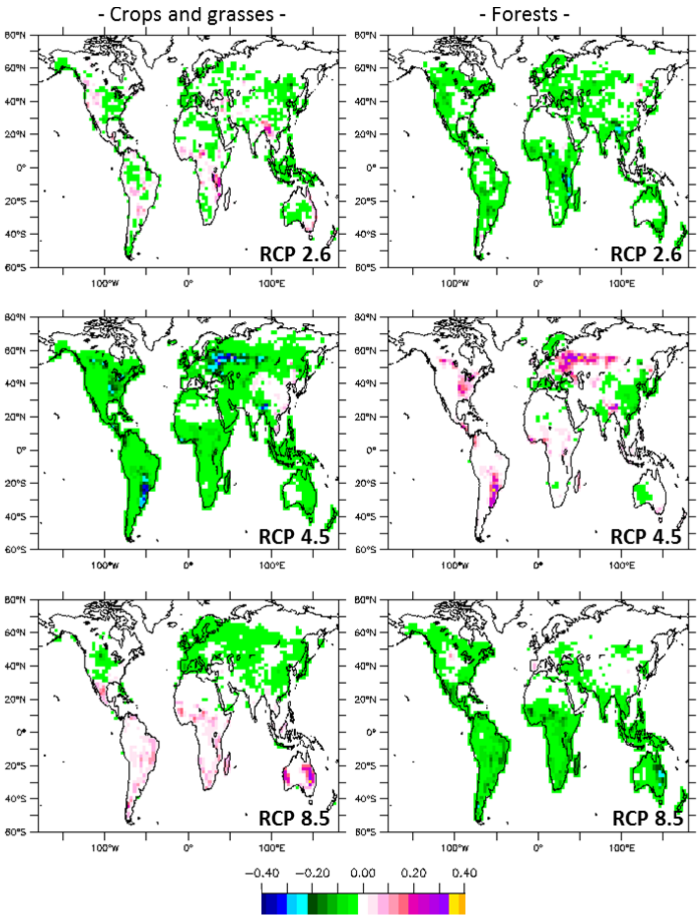

Figure 2. Vegetation fraction difference between 2050 and present-day for crops and grasses (left column), and forests (right column) according to the future RCP scenarios 2.6 (upper line), 4.5 (middle line) and 8.5 (lower line).

ACPD
15, 18459–18485, 2015

Impact of future land cover changes on HNO_3 and O_3 surface dry deposition

T. Verbeke et al.

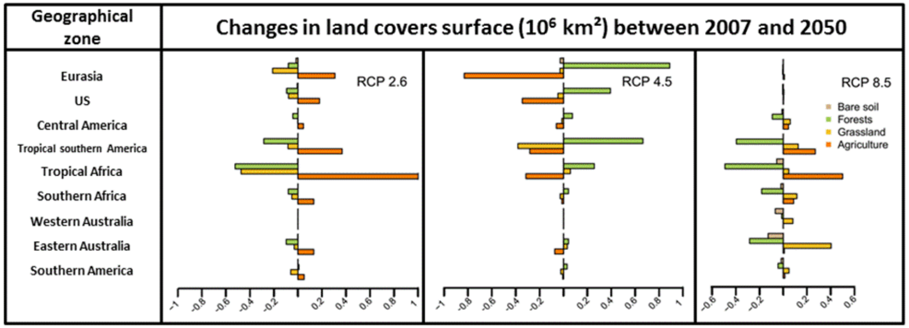

Figure 3. Changes between 2007 and 2050 in land-type surfaces (10^6 km^2) for the nine regions as illustrated in Fig. 1, in the case of forests (green), crops (orange), grasses (yellow) and bare soil (brown).

ACPD
15, 18459–18485, 2015

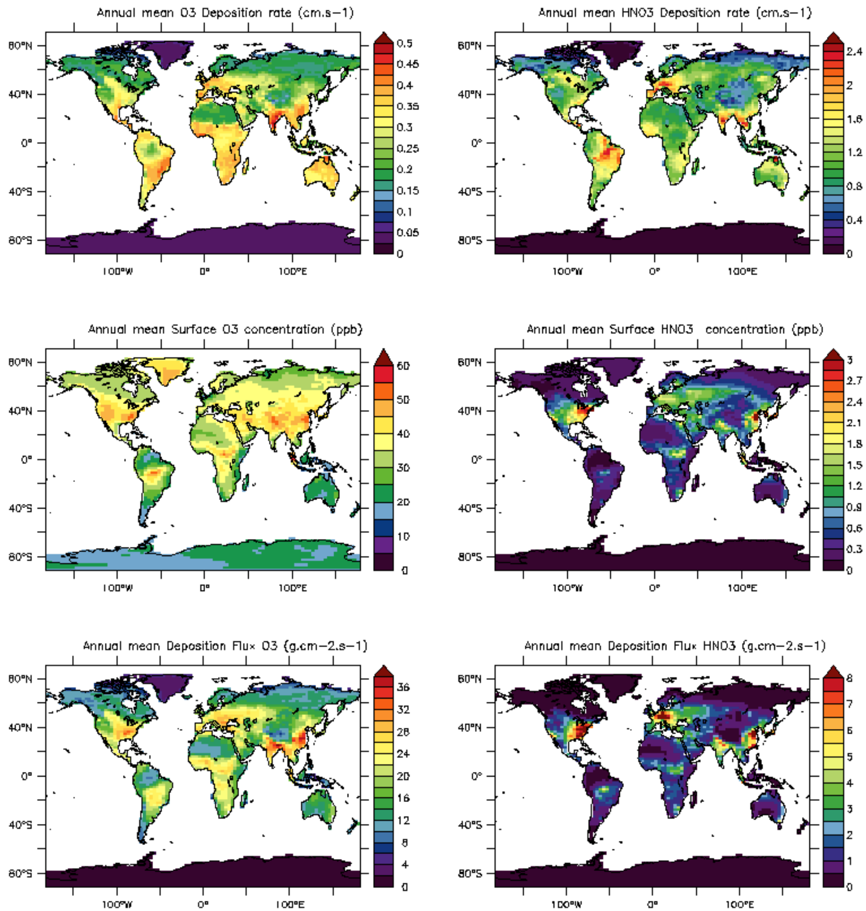

Figure 4. Annual average of dry deposition velocities (upper panel), surface concentrations (middle panel and deposition fluxes (lower panel) over continental surfaces ($cm\,s^{-1}$) for O_3 (left) and HNO_3 (right) for present-day as simulated by LMDz-INCA.

ACPD
15, 18459–18485, 2015

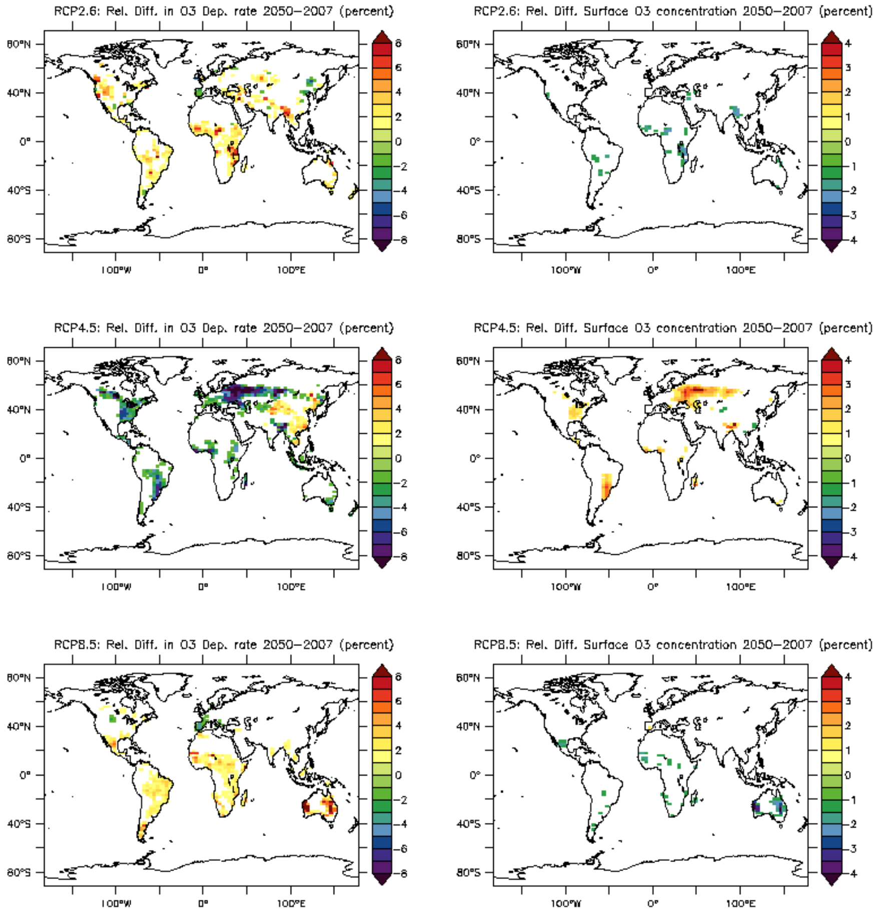

Figure 5. Annual mean changes (in relative value %) of Dry deposition velocity for O_3 between present-day and 2050 induced by the different LCC (left) and related surface ozone concentrations (right) for the three RCP scenarios. Values in the [−1; +1] % interval are not shown.

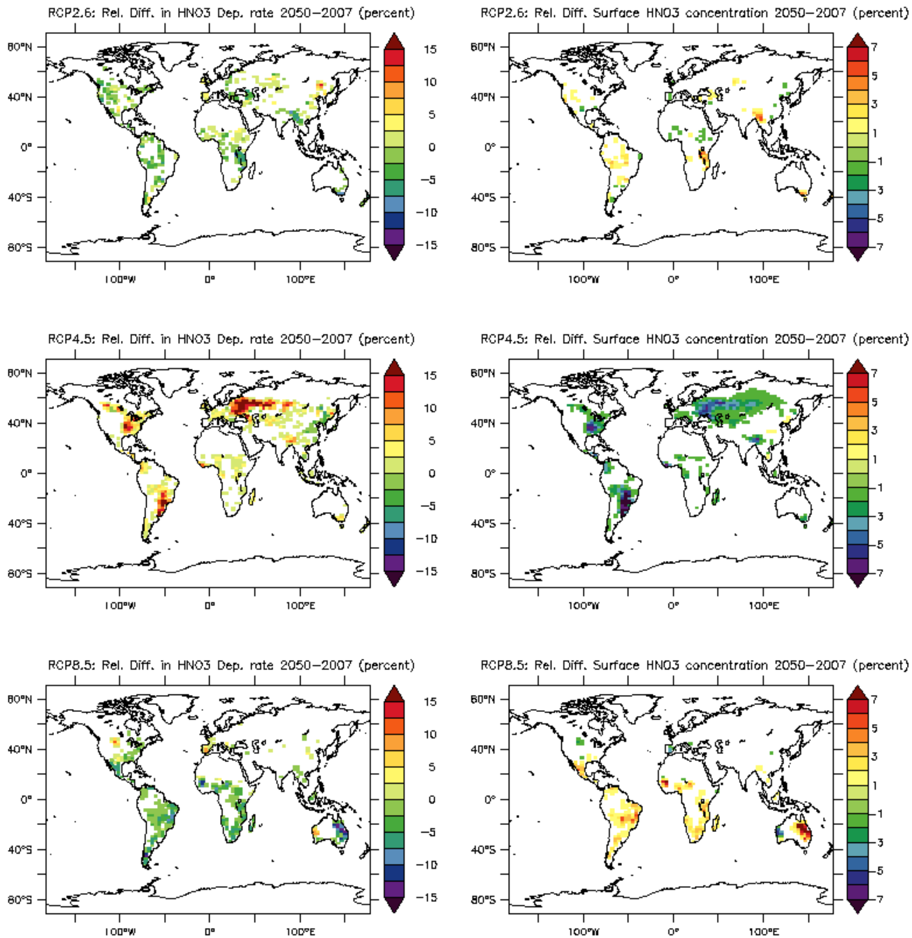

Figure 6. Same as Fig. 5 for HNO_3.

ACPD
15, 18459–18485, 2015

Impact of future land cover changes on HNO_3 and O_3 surface dry deposition

T. Verbeke et al.

Title Page
Abstract | Introduction
Conclusions | References
Tables | Figures
◀| |▶
◀ ▶
Back | Close
Full Screen / Esc
Printer-friendly Version
Interactive Discussion

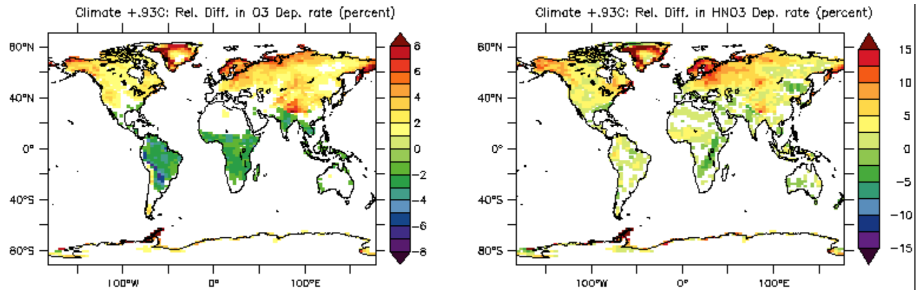

Figure 7. Future climate-induced impacts on dry deposition velocities (%) considering a 0.93 °C increase of global temperature.

ACPD
15, 18459–18485, 2015

Impact of future land cover changes on HNO_3 and O_3 surface dry deposition

T. Verbeke et al.